R-matrix calculation of integral and differential cross sections for low-energy electron-impact excitations of the N_2 molecule

Motomichi Tashiro* and Keiji Morokuma
Department of Chemistry, Emory University, 1515 Dickey Drive, Atlanta, Georgia 30322, USA
(Received 12 July 2006; revised manuscript received 17 November 2006; published 30 January 2007)

Low-energy electron-impact excitations of N_2 molecules are studied using the fixed-bond *R*-matrix method based on state-averaged complete active-space self-consistent-field orbitals. Thirteen target electronic states of N_2 are included in the model within a valence configuration interaction representation of the target states. Integrated as well as differential cross sections of the $A\ ^3\Sigma_u^+$, $B\ ^3\Pi_g$, $W\ ^3\Delta_u$, $B'\ ^3\Sigma_u^-$, $a'\ ^1\Sigma_u^-$, $a\ ^1\Pi_g$, $w\ ^1\Delta_u$, and $C\ ^3\Pi_u$ states are calculated and compared with the previous experimental measurements. These excitations, especially of the higher four states, have not been studied enough theoretically in the previous literature. In general, good agreements are observed both in the integrated and differential cross sections. However, some discrepancies are seen in the integrated cross sections of the $A^3\Sigma_u^+$ and $C\ ^3\Pi_u$ states, especially around a peak structure.

DOI: 10.1103/PhysRevA.75.012720 PACS number(s): 34.80.Gs

I. INTRODUCTION

Electron-impact excitation of nitrogen molecules plays an important role in atmospheric emission of planets and satellites such as the Earth, Titan, and Triton. For example, excitation of the $a\ ^1\Pi_g$ state and subsequent transitions to the ground $X\ ^1\Sigma_g^+$ state are responsible for the far-ultraviolet emissions of the Lyman-Birge-Hopfield system which are prominent in the airglow of the Earth's atmosphere [1]. Recently, Khakoo *et al.* [2] measured differential cross sections (DCS's) of electron-impact excitation of the N_2 molecule from the ground $X\ ^1\Sigma_g^+$ state to the eight lowest excited electronic states of $A\ ^3\Sigma_u^+$, $B\ ^3\Pi_g$, $W\ ^3\Delta_u$, $B'\ ^3\Sigma_u^-$, $a'\ ^1\Sigma_u^-$, $a\ ^1\Pi_g$, $w\ ^1\Delta_u$, and $C\ ^3\Pi_u$ states. Based on their differential cross-section data, Johnson *et al.* [3] derived integral cross sections (ICS's) for these electron-impact excitations. In general, their ICS's are smaller than the other experimental cross sections at low impact energies below 30 eV. These deviations may have some significance for the study of atmospheric emissions, because a mean kinetic energy of electrons at high altitudes is about 10 eV [4]. To shed light on this situation from a theoretical point of view, we perform *ab initio* *R*-matrix calculations of electron-impact excitations of N_2 molecules in this work.

Many previous experimental measurements have been focused on excitation to a specific electronic state. For example, Ajello and Shemansky [5] and Mason and Newell [6] measured ICS's for electron-impact excitation to the $a\ ^1\Pi_g$ state, whereas Poparic *et al.* [7], Zubek [8], and Zubek and King [9] measured cross sections for the $C\ ^3\Pi_u$ state. In addition to these works, Zetner and Trajmar [10] reported excitation cross sections to the $A\ ^3\Sigma_u^+$, $B\ ^3\Pi_g$, $W\ ^3\Delta_u$, and $a\ ^1\Pi_g$ states. So far, comprehensive measurements of the excitation to the eight lowest electronic states are limited to the three groups of Cartwright *et al.* [11], Brunger and Teubner [12], and Khakoo *et al.* [2]. The measurements of Brunger and Teubner [12] include excitation DCS's for the $E\ ^3\Sigma_g^+$ and $a''\ ^1\Sigma_g^+$ states in addition to the eight lowest excited states. The DCS's of Brunger and Teubner [12] and Khakoo *et al.* [2] were later converted to ICS's by Campbell *et al.* [13] and Johnson *et al.* [3], respectively. Detailed reviews of electron N_2 collisions can be found in Itikawa [14] and Brunger and Buckman [15].

Several groups have performed theoretical calculation of low-energy electron collisions with N_2 molecules. For example, Chung and Lin [16] employed the Born approximation to calculate excitation cross sections for the 11 target states including the $A\ ^3\Sigma_u^+$, $B\ ^3\Pi_g$, $W\ ^3\Delta_u$, $a\ ^1\Pi_g$, $w\ ^1\Delta_u$, and $C\ ^3\Pi_u$ states. Later, the same group of Holley *et al.* [17] calculated excitation ICS's for the $a\ ^1\Pi_g$ state using a two-state close-coupling method. Fliflet *et al.* [18] and Mu-Tao and McKoy [19] reported distorted-wave cross sections for excitation of the $A\ ^3\Sigma_u^+$, $B\ ^3\Pi_g$, $W\ ^3\Delta_u$, $w\ ^1\Delta_u$, $C\ ^3\Pi_u$, $E\ ^3\Sigma_g^+$, $b'\ ^1\Sigma_u^+$, and $c'\ ^1\Sigma_u^+$ states. In general, these approximate methods are expected to be accurate at high impact energies above 30 eV. However, a more elaborate method is required for precise comparison with experiments at low energies. Gillan *et al.* [20] calculated excitation ICS's for the $A\ ^3\Sigma_u^+$, $B\ ^3\Pi_g$, and $W\ ^3\Delta_u$ states using the fixed-nucleus *R*-matrix method. They included the four lowest target states in their *R*-matrix model, with target configuration interaction (CI) wave functions containing 2–13 Configuration State Function (CSF's). Their cross sections for the $A\ ^3\Sigma_u^+$ and $W\ ^3\Delta_u$ states agree well with the experimental results of Cartwright *et al.* [11]. However, ICS's for the $B\ ^3\Pi_g$ state deviate considerably from the experimental cross sections. Subsequently, they extended their *R*-matrix model to include the eight lowest valence states [21]. Their target CI wave functions were much improved from their previous work by employing valence active space description, resulting in 68–120 CSF's per target state. In their paper, the ICS's were shown for the $A\ ^3\Sigma_u^+$, $B\ ^3\Pi_g$, $W\ ^3\Delta_u$, and $B'\ ^3\Sigma_u^-$ states, while the DCS's were presented for only the $A\ ^3\Sigma_u^+$ state. Agreement with the ICS's of Cartwright *et al.* [11] is good for these four excited states. However, agreement is marginal at DCS level.

*Present address: Fukui Institute for Fundamental Chemistry, Kyoto University, Takano-Nishi-Hiraki-cho 34-4, Kyoto 606-8103, Japan. Electronic address: tashiro@fukui.kyoto-u.ac.jp

In this work, we study electron impact excitation of N_2 molecules by the fixed-nucleus R-matrix method as in our previous work on electron O_2 scatterings [22,23]. Although our theoretical treatment is similar to the previous work of Gillan *et al.* [21], more target states and partial waves of a scattering electron are included in the present work. The main purpose of this work is a comparison of ICS's as well as DCS's for the eight lowest excited states with the experimental results of Cartwright *et al.* [11], Brunger and Teubner [12], Campbell *et al.* [13], Khakoo *et al.* [2], and Johnson *et al.* [3]. This is because previous theoretical works have covered only a part of these eight excitations.

In this paper, details of the calculation are presented in Sec. II, and we discuss the results in Sec. III comparing our ICS's and DCS's with the previous theoretical and available experimental data. Then summary is given in Sec. IV.

II. THEORETICAL METHODS

The R-matrix method itself has been described extensively in the literature [24–26] as well as in our previous paper [22]. Thus we do not repeat general explanation of the method here. We used a modified version of the polyatomic programs in the UK molecular R-matrix codes [24]. These programs utilize Gaussian-type orbitals (GTO's) to represent target electronic states as well as a scattering electron. Although most of the previous R-matrix works on electron N_2 collisions have employed Slater-type orbitals (STO's), we select GTO's mainly because of simplicity of the input and availability of basis functions. In the R-matrix calculations, we have included 13 target states: $X\ ^1\Sigma_g^+$, $A\ ^3\Sigma_u^+$, $B\ ^3\Pi_g$, $W\ ^3\Delta_u$, $B'\ ^3\Sigma_u^-$, $a'\ ^1\Sigma_u^-$, $a\ ^1\Pi_g$, $w\ ^1\Delta_u$, $C\ ^3\Pi_u$, $E\ ^3\Sigma_g^+$, $a''\ ^1\Sigma_g^+$, $c\ ^1\Pi_u$, and $c'\ ^1\Sigma_u^+$. The potential energy curves of these target electronic states are shown in Fig. 1 for reference. These target states were represented by valence configuration interaction wave functions constructed by state-averaged complete active-space self-consistent-field (SA-CASSCF) orbitals. Note that some target states, $E\ ^3\Sigma_g^+$, $a''\ ^1\Sigma_g^+$, and $c'\ ^1\Sigma_u^+$, are Rydberg states and cannot be described adequately in the present valence active space. Inclusion of these states is intended to improve the quality of the R-matrix calculations by adding more target states in the model, as in our previous works [22,23] as well as other R-matrix works [27,28]. A test calculation was performed with an extra $4a_g$ orbital in the target orbital set. However, the target excitation energies as well as the excitation cross sections did not change much compared to the results with the valence orbital set described above. Also, removal of the $3b_{1u}$ orbital from the target active space did not affect the result much in our calculation. In this study, the SA-CASSCF orbitals were obtained by calculations with MOLPRO suites of programs [29]. The target orbitals were constructed from the [5s3p1d] level of basis set taken from Sarpal *et al.* [30]. In our fixed-bond R-matrix calculations, the target states were evaluated at the equilibrium bond length $R=2.068a_0$ of the N_2 $X\ ^1\Sigma_g^+$ ground electronic state. Although we also performed calculations with $R=2.100a_0$ as in the previous R-matrix calculation of Gillan *et al.* [21], the cross sections with $R=2.068a_0$ and $R=2.100a_0$ are almost the same. Thus, we will only show results with the equilibrium bond length of N_2 in the next section. The radius of the R-matrix sphere was chosen to be $10a_0$ in our calculations. In order to represent the scattering electron, we included diffuse Gaussian functions up to $l=5$, with nine functions for $l=0$, seven functions for $l=1$–3, and six functions for $l=4$ and 5. Exponents of these diffuse Gaussians were fitted using the GTOBAS program [31] in the UK R-matrix codes. In addition to these continuum orbitals, we included eight extra virtual orbitals, one for each symmetry.

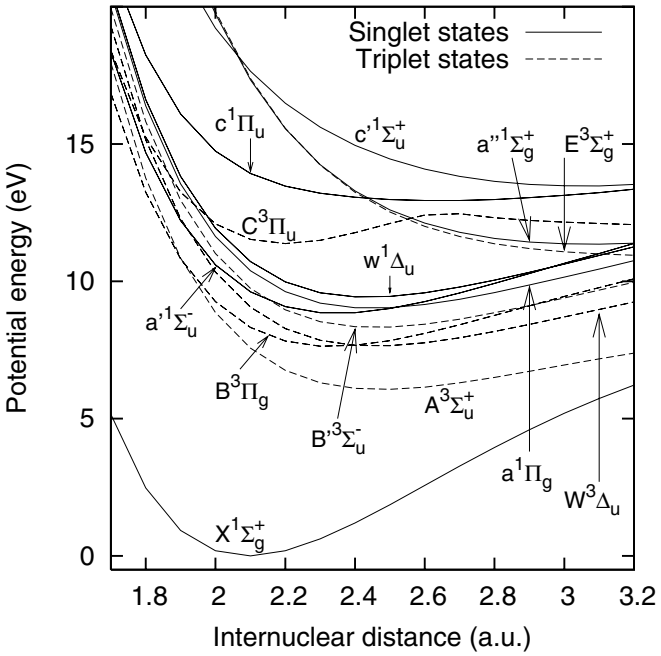

FIG. 1. Potential energy curves of the N_2 electronic states. The equilibrium distance of the $X\ ^1\Sigma_g^+$ state, $R=2.068a_0$, is used in our R-matrix calculations.

We constructed the 15-electron configurations from the orbitals listed in Table I. The CI target wave functions are composed of the valence orbitals in Table I with the $1a_g$ and $1b_{1u}$ orbitals kept doubly occupied. We have included three types of configurations in the calculation. The first type of configurations has the form

TABLE I. Division of the orbital set in each symmetry.

Symmetry	A_g	B_{2u}	B_{3u}	B_{1g}	B_{1u}	B_{3g}	B_{2g}	A_u
Valence	1-3a_g	1b_{2u}	1b_{3u}		1-3b_{1u}	1b_{3g}	1b_{2g}	
Extra virtual	4a_g	2b_{2u}	2b_{3u}	1b_{1g}	4b_{1u}	2b_{3g}	2b_{2g}	1a_u
Continuum	5-39a_g	3-35b_{2u}	3-35b_{3u}	2-17b_{1g}	5-37b_{1u}	3-18b_{3g}	3-18b_{2g}	2-17a_u

$$1a_g^2 1b_{1u}^2 \{2a_g 3a_g 1b_{2u} 1b_{3u} 2b_{1u} 3b_{1u} 1b_{3g} 1b_{2g}\}^{10}(^1A_g) \times \{5a_g \ldots 39a_g\}^1(^2A_g). \quad (1)$$

Here we assume that the total symmetry of this 15 electrons system is ^2A_g. The first 4 electrons are always kept in the $1a_g$ and $1b_{1u}$ orbitals; then, the next 10 electrons are distributed over the valence orbitals with the restriction of target-state symmetry, ^1A_g symmetry of the N_2 ground state in this case. The last electron, the scattering electron, occupies one of the diffuse orbitals, of a_g symmetry in this example. To complete the wave function with the total symmetry ^2A_g, we also have to include configurations with the other target states combined with diffuse orbitals having appropriate symmetry in the same way as in the example. The second type of configurations has the form

$$1a_g^2 1b_{1u}^2 \{2a_g 3a_g 1b_{2u} 1b_{3u} 2b_{1u} 3b_{1u} 1b_{3g} 1b_{2g}\}^{10}(^1A_g) \times \{4a_g\}^1(^2A_g), \quad (2)$$

where the scattering electron occupies a bound $4a_g$ extra virtual orbital, instead of the diffuse continuum orbitals in expression (1). As in Table I, we included one extra virtual orbital for each symmetry. The third type of configurations has the form

$$1a_g^2 1b_{1u}^2 \{2a_g 3a_g 1b_{2u} 1b_{3u} 2b_{1u} 3b_{1u} 1b_{3g} 1b_{2g}\}^{11}(^2A_g). \quad (3)$$

In this case, the last 11 electrons including the scattering electron are distributed over the valence orbitals with the restriction of ^2A_g symmetry. Note that the third type of configurations are crucial in description of N_2^- resonance states, which often have dominant contributions to the excitation cross sections. In this way, the number of configurations generated for a specific total symmetry is typically about 60 000, though the final dimension of the inner-region Hamiltonian is reduced to be about 600 by using the CI target contraction and prototype CI expansion method [32].

The *R*-matrix calculations were performed for all eight irreducible representations of the D_{2h} symmetry, A_g, B_{2u}, B_{3u}, B_{1g}, B_{1u}, B_{3g}, B_{2g}, and A_u, in doublet-spin multiplicity of the electron plus target system. DCS's were evaluated in the same way as in our previous paper [23].

III. RESULTS AND DISCUSSION

A. Excitation energies

Figure 1 shows the potential energy curves of all N_2 target states included in the present *R*-matrix model. These curves were obtained by the same SA-CASSCF method employed in our *R*-matrix calculation. Table II compares the excitation energies of the N_2 target states from the present calculation with the previous *R*-matrix results of Gillan *et al.* [21], multireference coupled-cluster results of Ben-Shlomo and Kaldor [33] as well as experimental values. Since these energies are evaluated at different internuclear distance, $2.068a_0$ in our case, $2.100a_0$ in Gillan *et al.* [21], and $2.074a_0$ in Ben-Shlomo and Kaldor [33], precise comparison is not so meaningful. However, deviations of excitation energies from the experimental values are less than 0.8 eV in our calculation, which is good considering the level of calculation. In terms of excitation energies, our calculation and the previous *R*-matrix calculation of Gillan *et al.* [21] have similar quality.

TABLE II. Comparison of the vertical excitation energies. The present results are shown with the previous works of Gillan *et al.* [21] and multireference coupled-cluster (MRCC) results of Ben-Shlomo and Kaldor [33] as well as experimental values quoted in Ben-Shlomo and Kaldor [33]. The unit of energy is eV.

State	This work	Previous *R*-matrix results	MRCC	Experimental values
$X\ ^1\Sigma_g^+$	0.00	0.00	0.00	0.00
$A\ ^3\Sigma_u^+$	7.89	7.63	7.56	7.75
$B\ ^3\Pi_g$	8.54	8.54	8.05	8.04
$W\ ^3\Delta_u$	9.38	9.11	8.93	8.88
$a\ ^1\Pi_g$	9.85	9.89	9.27	9.31
$B'\ ^3\Sigma_u^-$	10.06	9.83	9.86	9.67
$a'\ ^1\Sigma_u^-$	10.69	10.41	10.09	9.92
$w\ ^1\Delta_u$	11.01	10.74	10.54	10.27
$C\ ^3\Pi_u$	11.64		11.19	11.19

In addition to this good agreement of target energies with experimental results, N_2^+ energies are also well described in our SA-CASSCF calculation. In our calculation, N_2^+ $X\ ^2\Sigma_g^+$ and $A\ ^2\Pi_u$ states are located at 15.63 and 17.21 eV above N_2 $X\ ^2\Sigma_g^+$ state, respectively. Compared to the experimental values of 15.61 and 17.08 eV, our SA-CASSCF calculation gives good results. Note that the energy ordering of N_2^+ $X\ ^2\Sigma_g^+$ and $A\ ^2\Pi_u$ states is not well described in the Hartree-Fock level calculation; see Ermler and McLean [34], for example.

B. Integral cross sections

Figure 2 shows integral cross sections for electron impact excitation from the N_2 $X\ ^1\Sigma_g^+$ state to the $A\ ^3\Sigma_u^+$, $B\ ^3\Pi_g$, $W\ ^3\Delta_u$, and $B'\ ^3\Sigma_u^-$ states. In this figure, present results are compared with the previous *R*-matrix calculations of Gillan *et al.* [21], recent calculations of da Costa and Lima [35], experimental results of Cartwright *et al.* [11], Campbell *et al.* [13], and recent measurements of Johnson *et al.* [3]. Renormalized values of Cartwright *et al.* [11] are used as recommended by Trajmar *et al.* [36]. Figure 3 compares the present excitation cross sections of the $a'\ ^1\Sigma_u^-$, $a\ ^1\Pi_g$, $w\ ^1\Delta_u$, and $C\ ^3\Pi_u$ states with the previous experimental results of Cartwright *et al.* [11], Campbell *et al.* [13], and Johnson *et al.* [3]. For the $a\ ^1\Pi_g$–state cross sections, the recent calculations of da Costa and Lima [35] and other experimental values of Ajello and Shemansky [5], Zetner and Trajmar [10], and Mason and Newell [6] are included. For the $C\ ^3\Pi_u$–state cross sections, the experimental results of Zubek [8], Zubek and King [9], and Poparic *et al.* [7] are included.

Our excitation cross sections for the $A\ ^3\Sigma_u^+$ state have a resonance feature at approximately 12 eV as in the previous *R*-matrix results of Gillan *et al.* [21]. The N_2^- $^2\Pi_u$ resonance state is responsible for this peak structure. The

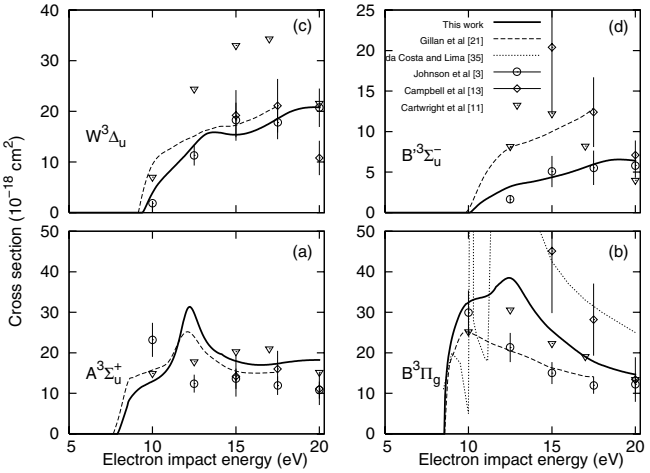

FIG. 2. Integral excitation cross sections of the $A\ ^3\Sigma_u^+$ [panel (a)], $B\ ^3\Pi_g$ [panel (b)], $W\ ^3\Delta_u$ [panel (c)], and $B'\ ^3\Sigma_u^-$ [panel (d)] states. Our results are shown as thick solid lines. For comparison, we include the previous R-matrix results of Gillan *et al.* [21], Schwinger multichannel results of da Costa and Lima [35], and the experimental cross sections of Cartwright *et al.* [11], Campbell *et al.* [13], and Johnson *et al.* [3].

main configuration of this resonance state is $1\pi_u^3 1\pi_g^2$. Other than the $^2\Pi_u$ symmetry partial cross sections, the $^2\Pi_g$ symmetry contributes to the ICS's as a smooth background component (not shown in the figure). Compared to the previous R-matrix cross sections, the peak at 12 eV is more pronounced in our case. Our results are slightly larger than theirs at 12–17.5 eV. Compared to the recent experimental results of Johnson *et al.* [3], our cross sections are about 50% larger at 12.5–20 eV, though 50% smaller at 10 eV. Also our calculation overestimates the results of Campbell *et al.* [13]; however, the results of Cartwright *et al.* [11] agree well with our results except at 12.5 eV. The position of the resonance peak depends rather strongly on the internuclear distance of N_2 molecule, which is 12.2 eV for $2.068a_0$ and 11.75 eV for $2.100a_0$ in our calculations. Thus, inclusion of vibrational motion may be necessary to resolve this discrepancy of the resonance peak.

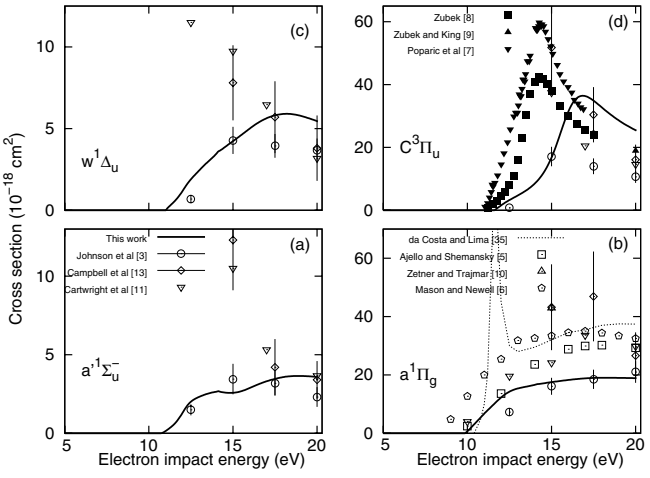

FIG. 3. Integral excitation cross sections of the $a'\ ^1\Sigma_u^-$ [panel (a)], $a\ ^1\Pi_g$ [panel (b)], $w\ ^1\Delta_u$ [panel (c)], and $C\ ^3\Pi_u$ [panel (d)] states. Our results are shown as thick solid lines. In addition to the experimental ICS's in Fig. 2, we include the results of Ajello and Shemansky [5], Zetner and Trajmar [10], Mason and Newell [6], Poparic *et al.* [7], Zubek [8], and Zubek and King [9].

Our excitation cross sections for the $B\ ^3\Pi_g$ state have a small bump at 12.8 eV, which is not evident in the previous R-matrix cross sections. The origin of this bump is the N_2^- $1\ ^2\Delta_g$ state, with main configuration of $3\sigma_g^1 1\pi_g^2$. Other than this bump, the ICS's are mostly composed of the $^2\Pi_g$ symmetry contribution and have a shape similar to the previous R-matrix results. The magnitude of our ICS's is about 50% larger than the previous results of Gillan *et al.* [21]. Recently, da Costa and Lima [35] calculated ICS's for the $B\ ^3\Pi_g$ state using the Schwinger multichannel method with the minimal orbital basis for the single-configuration interaction (MOBSCI) approach. There cross sections are much larger than our results above 12 eV. Also, there is a prominent peak around 10 eV in their ICS's, which does not exist in the R-matrix calculations. Compared to the experimental ICS's, our results agree well with the cross sections of Cartwright *et al.* [11], especially above 15 eV. However, the results of Campbell *et al.* [13] are much larger than ours. Recent measurements of Johnson *et al.* [3] agree better with the previous R-matrix calculation of Gillan *et al.* [21].

For the excitation cross sections for the $W\ ^3\Delta_u$ state, our results have a shape and magnitude similar to the previous R-matrix results. Most of our ICS's are composed of the $^2\Pi_g$ symmetry partial cross sections. Agreement with the experimental cross sections of Johnson *et al.* [3] is good in this case. The cross sections of Campbell *et al.* [13] agree well with our results at 15 and 17.5 eV, but their value is about half as much as our result at 20 eV. The results of Cartwright *et al.* [11] are about 2 times larger than our cross sections.

Our excitation cross sections for the $B'\ ^3\Sigma_u^-$ state are about half of the previous R-matrix cross sections of Gillan *et al.* [21]. Apart from this difference in magnitude, the shape of the cross sections is similar. Dominant component in these ICS's is the $^2\Pi_g$ symmetry partial cross sections, although the $^2\Pi_u$ symmetry also has certain contribution around 18–20 eV. Among three different experimental measurements, our results agree well with the results of Johnson *et al.* [3]. The experimental cross sections of other two groups are much larger than our results at 15 and 17.5 eV, and have a different energy dependence compared to the present calculation.

The situation of the excitation cross sections for the $a'\ ^1\Sigma_u^-$ state is similar to the case of the $B'\ ^3\Sigma_u^-$ state. The $^2\Pi_g$ and $^2\Pi_u$ symmetry partial cross sections contribute almost equally to the ICS's. Our cross sections roughly agree with the results of Johnson *et al.* [3], while the cross sections of Cartwright *et al.* [11], and Campbell *et al.* [13] at 15 eV are much larger than our result. The results of Cartwright *et al.* [11] and Campbell *et al.* [13] decrease as the impact energy increases from 15 to 20 eV; however, our cross sections increase mildly in this energy region.

In case of excitation to the $a\ ^1\Pi_g$ state, several other experimental results are available in addition to the measurements of Cartwright *et al.* [11], Campbell *et al.* [13], and Johnson *et al.* [3]. The cross-section profiles of Johnson *et al.*

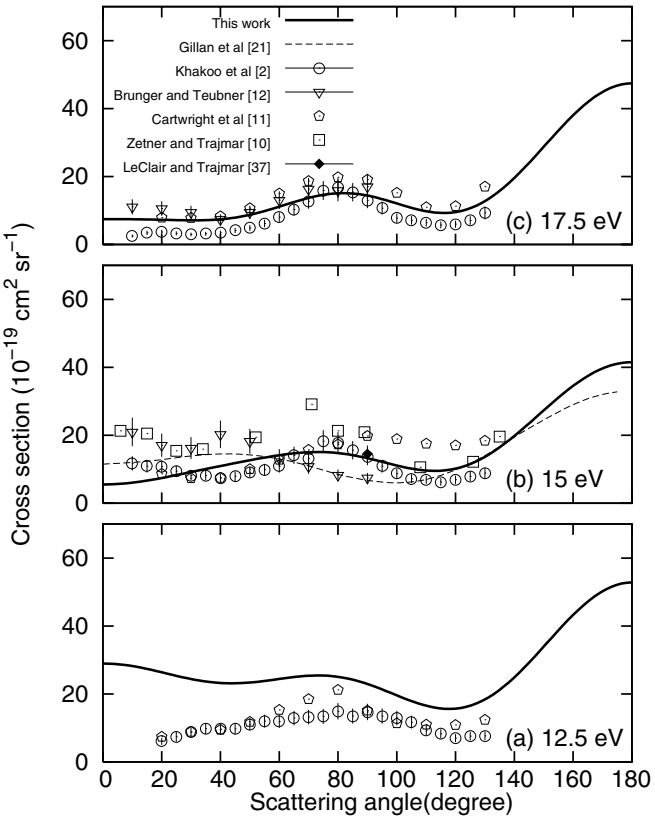

FIG. 4. Differential cross sections for electron-impact excitation from the N_2 $X\ ^1\Sigma_g^+$ state to the $A\ ^3\Sigma_u^+$ state. Electron-impact energy of (a) 12.5 eV, (b) 15 eV, and (c) 17.5 eV. The solid line represents our result. For comparison, we include the previous theoretical cross sections of Gillan *et al.* [21] and experimental results of Khakoo *et al.* [2], Brunger and Teubner [12], Cartwright *et al.* [11], Zetner and Trajmar [10], and LeClair and Trajmar [37].

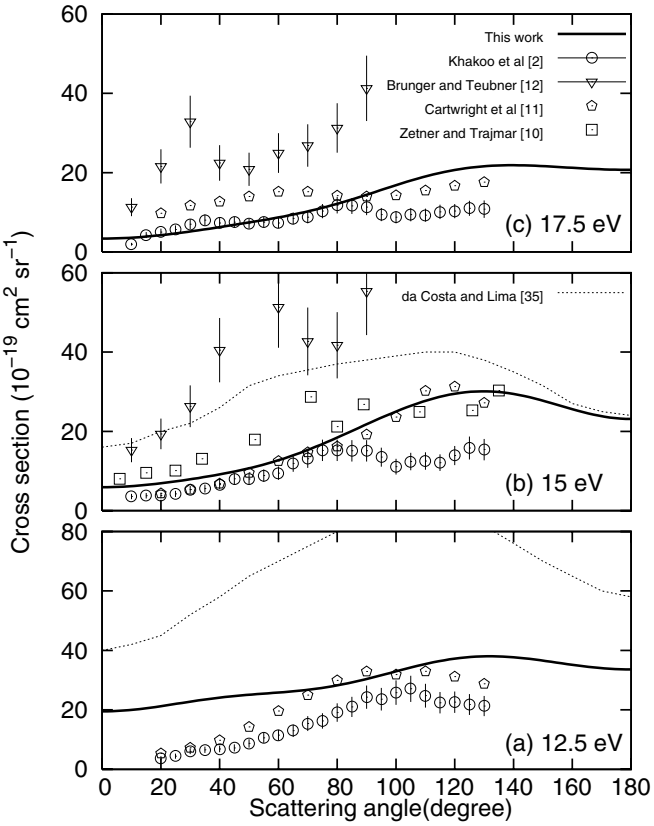

FIG. 5. Differential cross sections for electron-impact excitation from the N_2 $X\ ^1\Sigma_g^+$ state to the $B\ ^3\Pi_g$ state. Electron-impact energy of (a) 12.5 eV, (b) 15 eV, and (c) 17.5 eV. The results of Schwinger multichannel calculations by da Costa and Lima [35] are also shown in the panels. Other details are the same as in Fig. 4.

[3], Ajello and Shemansky [5], Cartwright *et al.* [11], and Mason and Newell [6] are similar to our ICS's. However, the magnitude of our cross sections is lower than the experimental values in most case except the cross sections of Johnson *et al.* [3]. At 15, 17.5, and 20 eV, agreement of our results with the cross sections of Johnson *et al.* [3] is very good, although our cross section at 12.5 eV is twice as large as their value. Note that there is no dominant symmetry contribution to the calculated ICS's. All partial cross sections contribute rather equally to the ICS's. Recent ICS's of da Costa and Lima [35] by the Schwinger multichannel method are also shown in panel (b) of Fig. 3. Their result has a sharp peak at 12 eV as in their calculation for the $B\ ^3\Pi_g$ state excitation. This difference between our and their results may come the from different number of target states considered in the scattering calculation. Only the $X\ ^1\Sigma_g^1$, $a\ ^1\Pi_g$, and $B\ ^3\Pi_g$ states were included in the calculations of da Costa and Lima. The other part of the cross-section profile is similar to the shape of our cross sections, although the magnitude of their cross sections are about twice as large as our results at 15–20 eV.

Our excitation cross section for the $w\ ^1\Delta_u$ state gradually increases as a function of energy from the threshold to the broad peak around 17.5 eV, then decreases toward 20 eV. In this case, agreement with the results of Johnson *et al.* [3] is not so good compared to the excitations of the $a\ ^1\Pi_g$ and $a'\ ^1\Sigma_u^-$ states. Our cross sections are about 50% larger than their values at 17.5 and 20 eV. At 15 eV, our results agree well with the cross section of Johnson *et al.* [3]; however, they are about 50% lower than the results of Cartwright *et al.* [11] and Campbell *et al.* [13]. In the calculated ICS's, the $^2\Pi_u$ symmetry partial cross section is a major component, with a minor contribution from the $^2\Pi_g$ symmetry.

The calculated excitation cross sections for the $C\ ^3\Pi_u$ state has a peak similar to the experimental results of Zubek [8] and Poparic *et al.* [7]. Although the shape of the cross sections is similar, the position of the cross-section peak is different from experimental results. In our case, it is located at about 17 eV, whereas corresponding peaks are located at 14 eV in the experimental cross sections. The height of the peak in our ICS's is lower than the experimental values of Zubek [8] and Poparic *et al.* [7]. It is unclear whether there is a cross-section peak in the experimental cross sections of Cartwright *et al.* [11], Campbell *et al.* [13], and Johnson *et al.* [3]. At least, it appears that they do not have a peak around 17 eV. The origin of this discrepancy in the cross section peak is uncertain, but may be related to the employment of the fixed-nucleus approximation or insufficiency of higher excited target states in the *R*-matrix model. The calculated ICS's are composed of the $^2\Sigma_u^+$ and $^2\Sigma_u^-$ symmetry

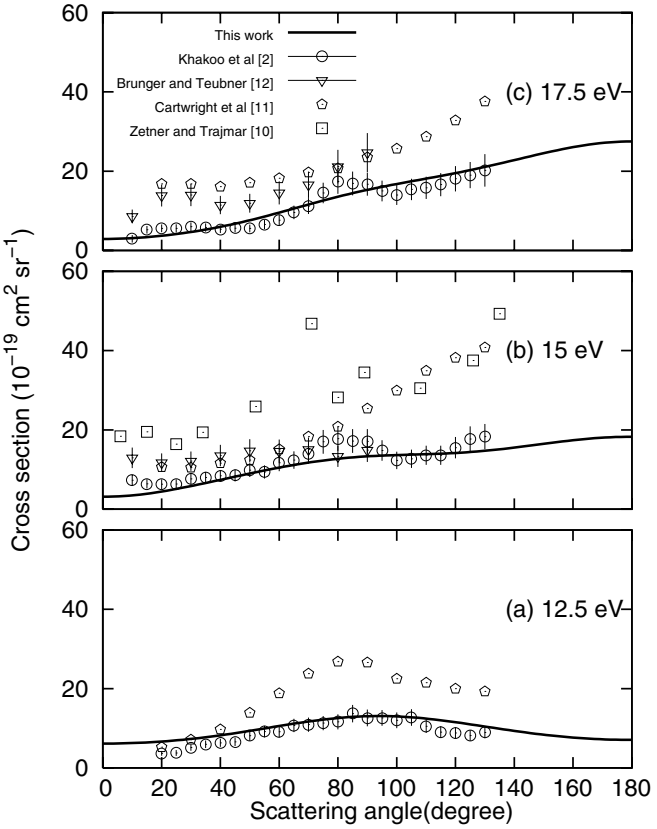

FIG. 6. Differential cross sections for electron-impact excitation from the N_2 $X\ ^1\Sigma_g^+$ state to the $W\ ^3\Delta_u$ state. Electron-impact energy of (a) 12.5 eV, (b) 15 eV, and (c) 17.5 eV. Other details are the same as in Fig. 4.

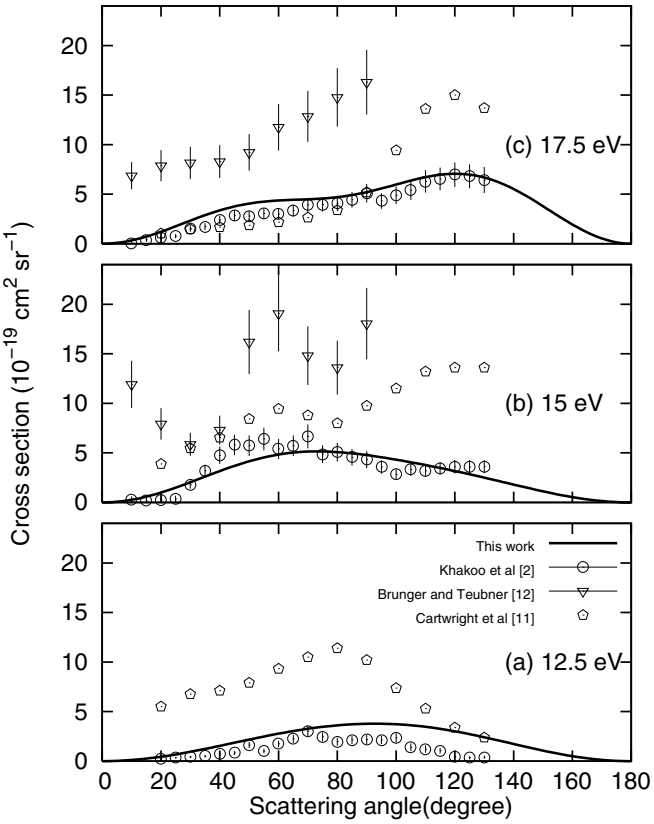

FIG. 7. Differential cross sections for electron-impact excitation from the N_2 $X\ ^1\Sigma_g^+$ state to the $B'\ ^3\Sigma_u^-$ state. Electron-impact energy of (a) 12.5 eV, (b) 15 eV, and (c) 17.5 eV. Other details are the same as in Fig. 4.

partial cross sections near the peak structure at 17 eV. The contribution of the $^2\Sigma_u^+$ symmetry is about 50% larger than the $^2\Sigma_u^-$ component. Other than these two symmetries, the $^2\Pi_g$ symmetry partial cross section contributes to the ICSs as a smooth background component.

C. Differential cross sections

Figure 4 shows calculated DCS's for excitation of the $A\ ^3\Sigma_u^+$ state with the experimental results of Khakoo *et al.* [2], Brunger and Teubner [12], Cartwright *et al.* [11], Zetner and Trajmar [10], LeClair and Trajmar [37] and the previous *R*-matrix DCS's of Gillan *et al.* [21]. Our DCS's at 12.5, 15, and 17.5 eV have a similar shape in common. They are enhanced in the backward direction and have a small dimple at 120° with a bump at 75°. At 17.5 eV, our cross sections are located between the experimental values of Khakoo *et al.* [2] and Cartwright *et al.* [11]. The profile of the experimental DCS's are reproduced well in our calculation. At 15 eV, our results agree better with the results of Khakoo *et al.* [2] compared to the other experiments. In the DCS's of the previous *R*-matrix calculation of Gillan *et al.* [21], a bump is located at 40° and a small dimple is located at 100°, which agree better with the experimental results of Brunger and Teubner [12]. In our calculation, these dimples and bumps are shifted toward the backward direction by 20°, and agreement with the results of Brunger and Teubner [12] is not so good. At 12.5 eV, our calculation overestimates the experimental results by a factor of 2. As seen in panel (a) of Fig. 2, this discrepancy is related to the existence of a resonance peak around 12.5 eV.

Figure 5 compares calculated excitation DCS's for the $B\ ^3\Pi_g$ state with the experimental and recent theoretical results. Our DCS's at 12.5, 15, and 17.5 eV have backward-enhanced feature with a broad peak at 130°. At 15 and 17.5 eV, our DCS's agree well with the results of Khakoo *et al.* [2] at forward direction below 80°. However, their DCS's are smaller than ours by a factor of 2 at 80°–130°. Agreement with the results of Cartwright *et al.* [11] at 15 eV is good at 20°–130°, although their DCS's are twice as large as our DCS's at 17.5 eV for low scattering angles. Because of a resonancelike feature at 12.5 eV as seen in panel (b) of Fig. 2, our results are larger than the experimental results at 12.5 eV. Recent Schwinger multichannel results of da Costa and Lima [35] are much larger than our DCS's at 12.5 and 15 eV. The deviation is especially large at 12.5 eV, which is possibly related to the difference in the excitation energies of the target state.

Figure 6 shows the excitation DCS's for the $W\ ^3\Delta_u$ state with the experimental cross sections. At 15 and 17.5 eV, our cross section gradually increases as a function of scattering angle, without noticeable bump or dip. At 12.5 eV, the shape of DCS's is nearly symmetric around 90°. Agreement with

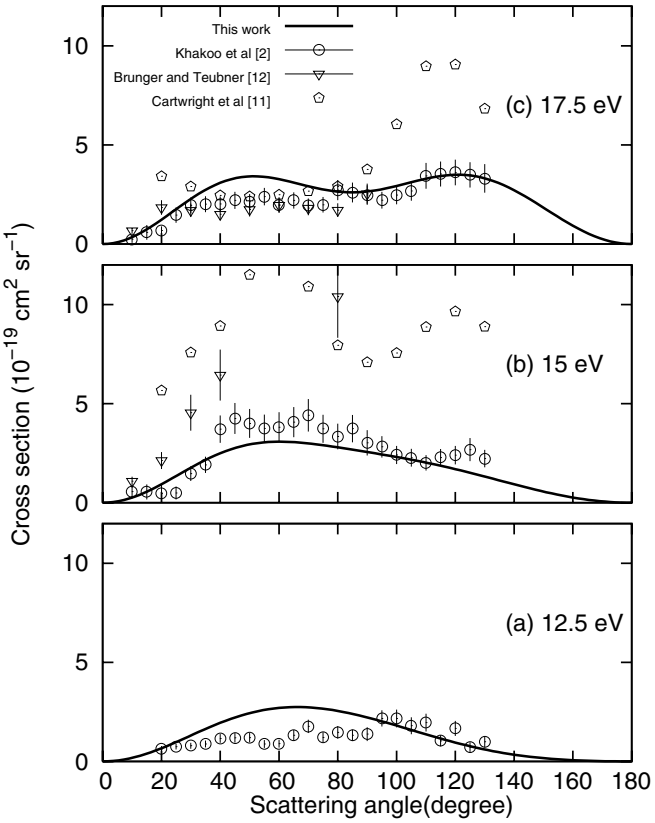

FIG. 8. Differential cross sections for electron-impact excitation from the N_2 $X\ ^1\Sigma_g^+$ state to the $a'\ ^1\Sigma_u^-$ state. Electron-impact energy of (a) 12.5 eV, (b) 15 eV, and (c) 17.5 eV. Other details are the same as in Fig. 4.

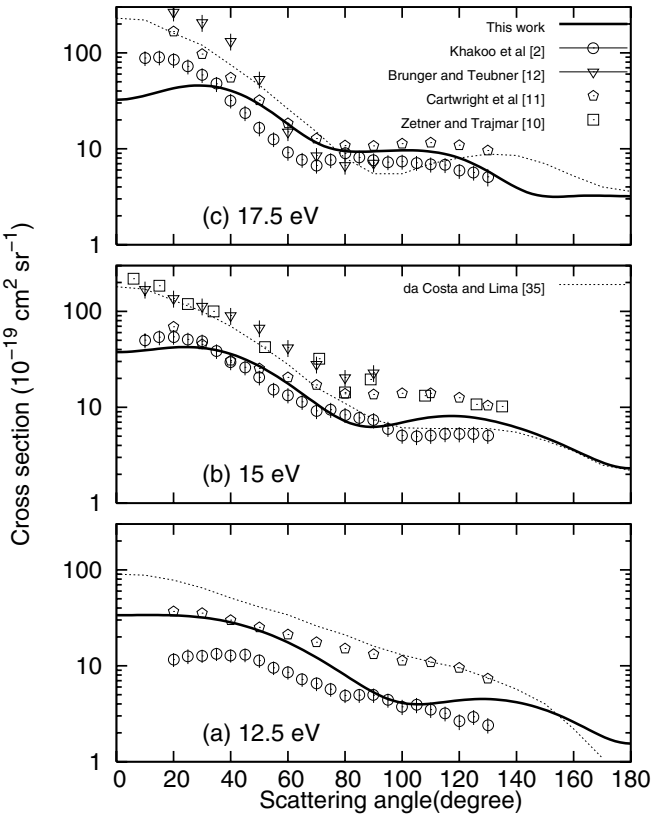

FIG. 9. Differential cross sections for electron-impact excitation from the N_2 $X\ ^1\Sigma_g^+$ state to the $a\ ^1\Pi_g$ state. Electron-impact energy of (a) 12.5 eV, (b) 15 eV, and (c) 17.5 eV. Note that the DCS's are shown in logarithmic scale. Other details are the same as in Fig. 4.

the experimental DCS's of Khakoo *et al.* [2] is good, although their results at 15 and 17.5 eV have more complex structure such as a small peak at 80°. Our DCS's are generally smaller than the other experimental results of Brunger and Teubner [12], Cartwright *et al.* [11], Zetner and Trajmar [10].

Excitation cross sections for the $B'\ ^3\Sigma_u^-$ state are shown in Fig. 7. Calculated DCS's decrease to be zero toward 0 and 180°, because of a selection rule associated with Σ^+-Σ^- transition [38,39]. Our DCS's have a broad single peak near 90° at 12.5 and 15 eV, whereas there are two broad peaks at 17.5 eV. The position of the right peak at 17.5 eV coincides with that of the experimental DCS's of Khakoo *et al.* [2] and Cartwright *et al.* [11], although the peak of Cartwright *et al.* [11] is much higher than ours. Our results agree well with the DCS's of Khakoo *et al.* [2] at 15 and 17.5 eV. However, their cross sections at 15 eV have a small dip at 100° and a small bump 60°, which do not exist in our results. At 12.5 eV, our cross sections are slightly larger than the results of Khakoo *et al.* [2]. On the whole, agreement with the other experimental results of Brunger and Teubner [12] and Cartwright *et al.* [11] is not good.

Figure 8 shows the excitation DCS's for the $a'\ ^1\Sigma_u^-$ state. Because of the Σ^+-Σ^- selection rule, DCS's at 0 and 180° become zero as in the case of the $B'\ ^3\Sigma_u^-$-state DCS's. Calculated DCSs have a broad single peak near 60° at 12.5 and 15 eV. At 17.5 eV, there are two broad peaks at 50° and 120°. Although there is slight overestimation of DCS's near 50°–60°, our DCS's agree marginally with the results of Khakoo *et al.* [2]. Agreement with the other experimental results is not good except low scattering angles at 17.5 eV.

Figure 9 compares our excitation DCS's for the $a\ ^1\Pi_g$ state with the experimental cross sections. Because of large variation of the DCS's, the cross sections are shown in logarithmic scale. Calculated DCS's are strongly forward enhanced, which is consistent with all experimental results shown in the figure. Our DCS's at 12.5 eV have a small dip around 100°, which moves forward to 85° at 15 eV and 75° at 17.5 eV. This behavior roughly agrees with the results of Cartwright *et al.* [11] and Khakoo *et al.* [2]. At 15 eV, our DCS's agree better with the results of Khakoo *et al.* [2] than the other experimental DCS's. At 17.5 eV, the results of Cartwright *et al.* [11] are closer to our DCS's at scattering angles above 40°. Below 40°, our calculation significantly underestimates the experimental DCS's. Our results at 12.5 eV are located between the DCS's of Cartwright *et al.* [11] and Khakoo *et al.* [2]; however, the shape of the DCS's is similar to their results. The shapes of DCS's calculated by da Costa and Lima [35] are similar to our results. However, their cross sections are larger than our results at low scattering angles below 80°, where their results agree better with the experimental DCS's of Brunger and Teubner [12] and Zetner and Trajmar [10].

Figure 10 shows calculated excitation DCS's for the $w\ ^1\Delta_u$ state with the experimental cross sections. Our DCS's

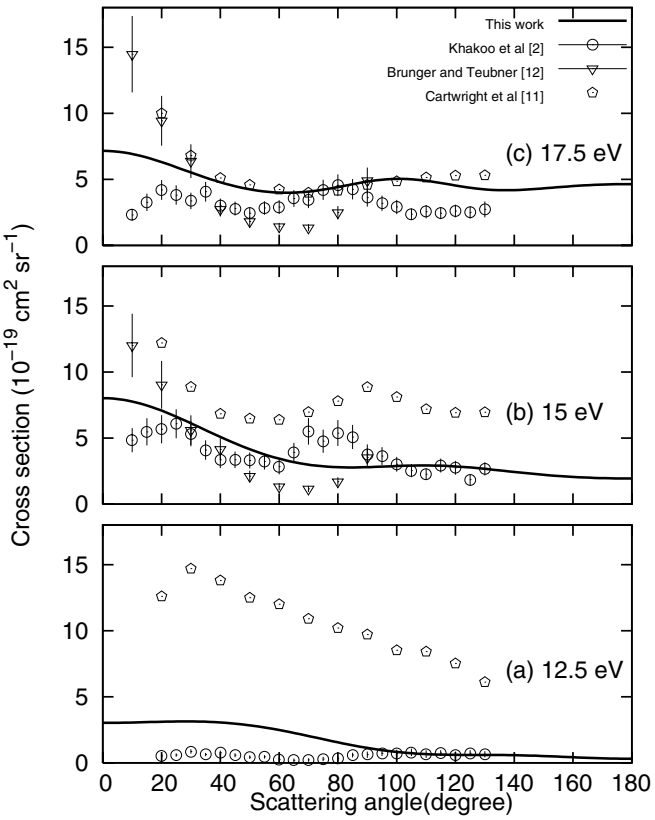

FIG. 10. Differential cross sections for electron-impact excitation from the N_2 $X\,^1\Sigma_g^+$ state to the $w\,^1\Delta_u$ state. Electron-impact energy of (a) 12.5 eV, (b) 15 eV, and (c) 17.5 eV. Other details are the same as in Fig. 4.

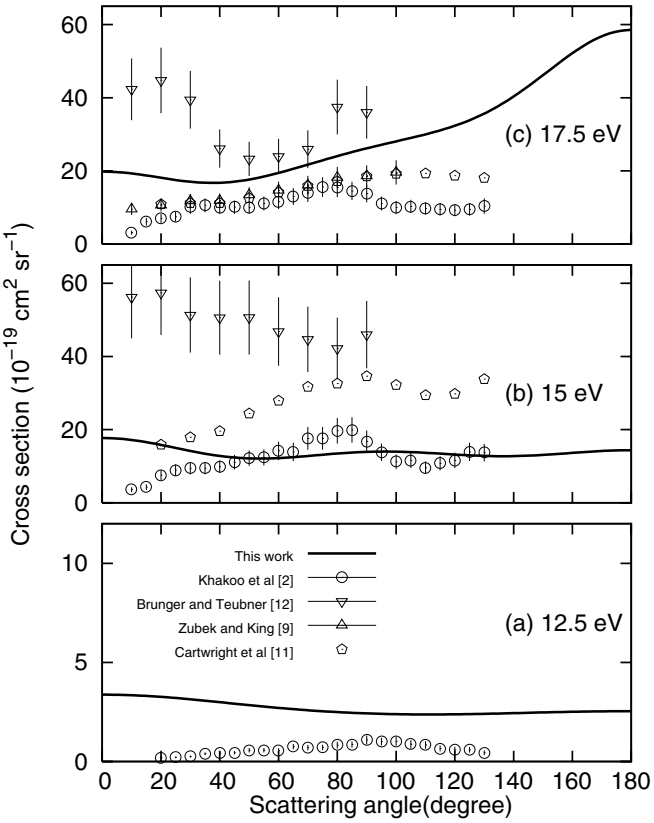

FIG. 11. Differential cross sections for electron-impact excitation from the N_2 $X\,^1\Sigma_g^+$ state to the $C\,^3\Pi_u$ state. Electron-impact energy of (a) 12.5 eV, (b) 15 eV, and (c) 17.5 eV. The experimental DCS's of Zubek and King [9] are added. Other details are the same as in Fig. 4.

are enhanced in the forward direction as in the case of the $a\,^1\Pi_g$ state. However, magnitude of the enhancement is much smaller than that of the $a\,^1\Pi_g$ state. Agreement with the DCS's of Cartwright *et al.* [11] is good at 17.5 eV except at low scattering angles below 20°. At 12.5 and 15 eV, their results are much larger than our DCS's. At 15 eV, our DCS's agree marginally with the results of Khakoo *et al.* [2], although details of the DCS profile are different. Their results are smaller than ours at 17.5 and 12.5 eV. The discrepancy is especially large for forward scattering at 12.5 eV.

Figure 11 shows excitation DCS's for the $C\,^3\Pi_u$ state with the experimental cross sections of Khakoo *et al.* [2], Brunger and Teubner [12], Zubek and King [9], and Cartwright *et al.* [11]. Calculated DCS profiles are almost flat at 12.5 and 15 eV, whereas they are enhanced in the backward direction at 17.5 eV. Below 90°, the slope of the calculated DCS's at 17.5 eV is similar to the results of Khakoo *et al.* [2], Zubek and King [9], and Cartwright *et al.* [11], though our results are about 50% larger than their DCS's. In general, our results do not agree well with the experimental DCS's. Although the ICS of Khakoo *et al.* [2] at 15 eV agrees well our result as shown in panel (d) of Fig. 3, the angular dependence of the cross sections appears to be different.

D. Discussion

The excitation ICS's of the $B\,^3\Pi_g$ state, shown in panel (b) of Fig. 2, have a small bump around 13 eV. However, there is no such structure in the previous *R*-matrix ICS's of Gillan *et al.* [21]. The origin of this bump in our calculation is the N^-_2 $1\,^2\Delta_g$ state, with a main configuration of $3\sigma_g^1 1\pi_g^2$. The existence of the N^-_2 $1\,^2\Delta_g$ state can also be verified by usual CASSCF calculation of N_2^- with valence active space ignoring continuum orbitals. In MOLPRO calculations, the energy of the $1\,^2\Delta_g$ state is 15.7 eV. Since diffuse continuum orbitals are added in the *R*-matrix calculation, the energy of the state is stabilized to be 12.8 eV in the present scattering calculation. In the same way, the N_2^- $^2\Pi_u$ $(1\pi_u^3 1\pi_g^2)$ resonance peak in the $A\,^3\Sigma_u^+$ excitation ICS's can be verified by the usual CASSCF calculations. In MOLPRO calculations, it is located at 14.7 eV, whereas the position of the resonance is stabilized to be 12.2 eV in our *R*-matrix scattering calculation. It is unclear why the bump in the ICS's of the $B\,^3\Pi_g$ state is not evident in the previous *R*-matrix cross sections of Gillan *et al.* [21]. Some details of the *R*-matrix calculations are different in their calculation and ours; e.g., they used hybrid orbitals with Slater-type functions, whereas we employed SA-CASSCF orbitals with Gaussian-type functions. These differences may contribute to the difference in magnitude of the $^2\Delta_g$ partial cross section.

In this study, we employed the fixed-nucleus (FN) approximation. As we can see in Fig. 1, equilibrium bond lengths of the excited N_2 states are longer than that of the ground state. Thus, in principle, it would be desirable to

include the effect of nuclear motion in the *R*-matrix calculation. Use of the FN approximation may be responsible for several discrepancies between our calculation and experiments, including bumps in the ICS's of the $A\ ^3\Sigma_u^+$ and $B\ ^3\Pi_g$ states and the position of the peak in the ICS's of the $C\ ^3\Pi_u$ state. Although the calculated DCS's agree very well with experimental results in general, our DCS's of the $A\ ^3\Sigma_u^+$, $B\ ^3\Pi_g$, $w\ ^1\Delta_u$, and $C\ ^3\Pi_u$states at 12.5 eV are 2–4 times larger than experimental results. These deviations in the near-threshold DCS's can also be related to the FN approximation. In spite of these discrepancies, good agreements are observed between our calculation and experiments in most ICS and DCS cases as we can see in the figures. Agreements with the recent experimental results of Khakoo *et al.* [2] and Johnson *et al.* [3] are especially impressive. It is possible to include nuclear motion in the *R*-matrix formalism through vibrational averaging of *T*-matrix elements or the nonadiabatic *R*-matrix method, though application of these methods will be a difficult task in the presence of many target electronic states. In the future, we plan to perform the *R*-matrix calculation with these methods including nuclear motion.

IV. SUMMARY

We have investigated electron impact excitations of N_2 molecules using the fixed-bond *R*-matrix method which includes 13 target electronic states: $X\ ^1\Sigma_g^+$, $A\ ^3\Sigma_u^+$, $B\ ^3\Pi_g$, $W\ ^3\Delta_u$, $B'\ ^3\Sigma_u^-$, $a'\ ^1\Sigma_u^-$, $a\ ^1\Pi_g$, $w\ ^1\Delta_u$, $C\ ^3\Pi_u$, $E\ ^3\Sigma_g^+$, $a''\ ^1\Sigma_g^+$, $c\ ^1\Pi_u$, and $c'\ ^1\Sigma_u^+$. These target states are described by CI wave functions in the valence CAS space, using SA-CASSCF orbitals. Gaussian-type orbitals were used in this work, in contrast to the STO's in the previous *R*-matrix works. We have obtained integral cross sections as well as differential cross sections of excitations to the $A\ ^3\Sigma_u^+$, $B\ ^3\Pi_g$, $W\ ^3\Delta_u$, $B'\ ^3\Sigma_u^-$, $a'\ ^1\Sigma_u^-$, $a\ ^1\Pi_g$, $w\ ^1\Delta_u$, and $C\ ^3\Pi_u$ states, which have been studied a lot experimentally but not enough theoretically before. In general, good agreements are observed both in the integrated and differential cross sections, which is encouraging for further theoretical and experimental studies in this field. However, some discrepancies are seen in the integrated cross sections of the $A\ ^3\Sigma_u^+$ and $C\ ^3\Pi_u$ states, especially around a peak structure. Also, our DCS's do not agree well with the experimental results at low impact energy of 12.5 eV, compared to the higher energies of 15 and 17.5 eV. These discrepancies may be related to the fixed-nucleus approximation or insufficiency of higher excited target states in the *R*-matrix model.

ACKNOWLEDGMENTS

The work of M.T. is supported by the Japan Society for the Promotion of Science. The present research is supported in part by a grant from the Air Force Office of Scientific Research: the Advanced High-Energy Closed-Cycle Chemical Lasers project (No. F49620-02-1-0357).

[1] R. R. Meier, Space Sci. Rev. **58**, 1 (1991).
[2] M. A. Khakoo, P. V. Johnson, I. Ozkay, P. Yan, S. Trajmar, and I. Kanik, Phys. Rev. A **71**, 062703 (2005).
[3] P. V. Johnson, C. P. Malone, I. Kanik, K. Tran, and M. A. Khakoo, J. Geophys. Res., [Space Phys.] **110**, 11311 (2005).
[4] R. P. Wayne, *Chemistry of Atmospheres*, 3rd ed. (Oxford University Press, New York, 2000).
[5] J. M. Ajello and D. E. Shemansky, J. Geophys. Res., [Space Phys.] **90**, 9845 (1985).
[6] N. J. Mason and W. R. Newell, J. Phys. B **20**, 3913 (1987).
[7] G. Poparic, M. Vicic, and D. S. Belic, Chem. Phys. **240**, 283 (1999).
[8] M. Zubek, J. Phys. B **27**, 573 (1994).
[9] M. Zubek and G. C. King, J. Phys. B **27**, 2613 (1994).
[10] P. W. Zetner and S. Trajmar, in *Abstracts of the Fifteenth International Conference on the Physics of Electronic and Atomic Collisions, Brighton*, edited by J. Geddes, H. B. Gilbody, A. E. Kingston, and C. J. Latimer (Queen's University, Belfast, 1987) (tabulated data were taken from Brunger and Buckman [15]).
[11] D. C. Cartwright, A. Chutjian, S. Trajmar, and W. Williams, Phys. Rev. A **16**, 1013 (1977).
[12] M. J. Brunger and P. J. O. Teubner, Phys. Rev. A **41**, 1413 (1990).
[13] L. Campbell, M. J. Brunger, A. M. Nolan, L. J. Kelly, A. B. Wedding, J. Harrison, P. J. O. Teubner, D. C. Cartwright, and B. McLaughlin, J. Phys. B **34**, 1185 (2001).
[14] Y. Itikawa, J. Phys. Chem. Ref. Data **35**, 31 (2006).
[15] M. J. Brunger and S. J. Buckman, Phys. Rep. **357**, 215 (2002).
[16] S. Chung and C. C. Lin, Phys. Rev. A **6**, 988 (1972).
[17] T. K. Holley, S. Chung, C. C. Lin, and E. T. P. Lee, Phys. Rev. A **24**, 2946 (1981).
[18] A. W. Fliflet, V. Mckoy, and T. N. Rescigno, J. Phys. B **12**, 3281 (1979).
[19] Lee Mu-Tao and V. Mckoy, Phys. Rev. A **28**, 697 (1983).
[20] C. J. Gillan, C. J. Noble, and P. G. Burke, J. Phys. B **23**, L407 (1990).
[21] C. J. Gillan, J. Tennyson, B. M. McLaughlin, and P. G. Burke, J. Phys. B **29**, 1531 (1996).
[22] M. Tashiro, K. Morokuma, and J. Tennyson, Phys. Rev. A **73**, 052707 (2006).
[23] M. Tashiro, K. Morokuma, and J. Tennyson, Phys. Rev. A **74**, 022706 (2006).
[24] L. A. Morgan, J. Tennyson, and C. J. Gillan, Comput. Phys. Commun. **114**, 120 (1998).
[25] P. G. Burke and J. Tennyson, Mol. Phys. **103**, 2537 (2005).
[26] J. D. Gorfinkiel, A. Faure, S. Taioli, C. Piccarreta, G. Halmova, and J. Tennyson, Eur. Phys. J. D **35**, 231 (2005).
[27] C. J. Noble and P. G. Burke, Phys. Rev. Lett. **68**, 2011 (1992).
[28] K. Higgins, C. J. Noble, and P. G. Burke, J. Phys. B **27**, 3203 (1994).
[29] H.-J. Werner *et al.*, MOLPRO, version 2002.6, a package of *ab initio* programs.
[30] B. K. Sarpal, K. Pfingst, B. M. Nestmann, and S. D. Peyerim-

hoff, J. Phys. B **29**, 857 (1996).
[31] A. Faure, J. D. Gorfinkiel, L. A. Morgan, and J. Tennyson, Comput. Phys. Commun. **144**, 224 (2002).
[32] J. Tennyson, J. Phys. B **29**, 1817 (1995).
[33] S. B. Ben-Shlomo and U. Kaldor, J. Chem. Phys. **92**, 3680 (1990).
[34] W. C. Ermler and A. D. McLean, J. Chem. Phys. **73**, 2297 (1980).
[35] R. F. da Costa and M. A. P. Lima, Int. J. Quantum Chem. **106**, 2664 (2006).
[36] S. Trajmar, D. F. Register, and A. Chutjian, Phys. Rep. **97**, 221 (1983).
[37] L. R. LeClair and S. Trajmar, J. Phys. B **29**, 5543 (1996).
[38] W. A. Goddard III , D. L. Huestis, D. C. Cartwright, and S. Trajmar, Chem. Phys. Lett. **11**, 329 (1971).
[39] D. C. Cartwright, S. Trajmar, W. Williams, and D. L. Huestis, Phys. Rev. Lett. **27**, 704 (1971).